Hindawi
Wireless Communications and Mobile Computing
Volume 2022, Article ID 3167717, 13 pages
https://doi.org/10.1155/2022/3167717

Research Article

Evaluation of Weighted Nuclear Norm Minimization Algorithm for Ultrasound Image Denoising

Shaik Mahaboob Basha,[1,2] **Aloísio Vieira Lira Neto**,[2] **José Wally M. Menezes**,[2] **Samia Allaoua Chelloug**,[3] **Mohamed Abd Elaziz**,[4,5,6] **and Victor Hugo C. de Albuquerque**[7]

[1]*Department of Electronics and Communication Engineering, Geethanjali Institute of Science and Technology, Nellore, India*
[2]*Graduation Program in Telecommunication Engineering, Federal Institute of Ceará, Fortaleza, CE, Brazil*
[3]*Department of Information Technology, College of Computer and Information Sciences, Princess Nourah bint Abdulrahman University, P.O.Box 84428, Riyadh 11671, Saudi Arabia*
[4]*Faculty of Computer Science and Engineering, Galala University, Suez 435611, Egypt*
[5]*Artificial Intelligence Research Center (AIRC), Ajman University, Ajman 346, UAE*
[6]*Department of Mathematics, Faculty of Science, Zagazig University, Zagazig 44519, Egypt*
[7]*Department of Teleinformatics Engineering, Federal University of Ceará, Fortaleza, CE, Brazil*

Correspondence should be addressed to Shaik Mahaboob Basha; mohisin7@yahoo.co.in and Samia Allaoua Chelloug; sachelloug@pnu.edu.sa

Received 26 March 2022; Accepted 22 April 2022; Published 27 May 2022

Academic Editor: Kuruva Lakshmanna

Anatomical structures manifested in ultrasound (US) images are crucial in efficient disease diagnosis. This modality has been used to analyze different tissue properties, such as blood flow, in-depth tissue motion, and elasticity. Analysis of these US images is posing a critical challenge, as these images are corrupted with noise primarily induced during acquisition. The biological structures intended to be investigated need to be detected, enhanced, and preserved during image processing-based diagnosis. US-based common carotid artery (CCA) images were considered in this study, and five denoising techniques were explored for noise removal after converting the images to grayscale to identify efficient preprocessing for effective diagnosis. Furthermore, filtered images were subjected to different entropy-inspired segmentation for qualitative validation and to segment the CCA. The objective of this paper is a deliberate attempt to investigate the possible use of edge- and structure-preserving filtering techniques to segment tissues of interest. The weighted nuclear norm minimization (WNNM) approach appears to be effective in removing noise and simultaneously preserving the sensitive structures. Quantitative validation with peak signal to noise ratio (PSNR), structural symmetry index measure (SSIM), and feature similarity index measure (FSIM) found to be 27.84 ± 1.04 dB; 0.76 ± 0.01 and 0.87 ± 0.01 were observed to be superiorly high with WNNM filtering. The input image and the filtered image histograms are also compared for qualitative validation. The key finding in this study can be attributed to the ability to remove noise from US images corrupted with noise while preserving the anatomical details. Furthermore, it can be hypothesized that the anatomical structures under the influence of noise can be efficiently preprocessed and can be fed as a viable image towards segmentation followed by recognition and morphological inference.

1. Introduction

Early detection of cardiovascular diseases (CVDs) by means of suitable formulation of image-based biomarkers can lead to effective diagnosis systems. Discerning several structures, including intima-media thickness (IMT), in US-based CCA images is challenging due to the inherently low contrast of the respective structures. Morphological information related to IMT is linked to the pathology of stroke reported to be found in elderly adults. Effective edge detection and

segmentation approaches are needed in efficient IMT determination. Accurate IMT determination is crucial for determining and evaluating the potential risk of stroke. Efficient preprocessing of the ultrasound images can also aid in segmenting the object prior to recognition. Hence, a preprocessing technique that preserves the anatomical structures and helps in the following image processing stages can be effective in designing efficient pipelines for ultrasound image-based diagnosis. In this paper, an attempt was made to investigate the performances of the structure-preserving WNNM filtering technique, edge-preserving ADF, and conventional filtering techniques such as Gaussian filtering, median filtering, and average filters.

The layout and organization of this paper areas follows. Section 2 presents a succinct literature review of existing denoising mechanisms. Section 3 considers the proposed methodology, while Section 4 provides a detailed discussion and critique of the simulation results and summary of the work. Section 5 encompasses the conclusion and the future scope of denoising mechanisms.

2. Literature Review

US images have proven to be very effective in diagnosing several critical diseases. US imaging is popularly used to visualize biological structures such as the heart, carotid artery, abdomen, breast, and blood vessels [1–4]. The primary challenges posed by ultrasound images in medical image analysis are the presence of anatomical structures surrounded by grainy noise resembling the background. Recognizing the specific anatomical structure and associated diagnostic information is highly challenging, and effective preprocessing can help accomplish the task. Identifying edges representing anatomical structures is a critical preprocessing stage that can aid in several important tasks, such as object detection and segmentation [5, 6]. Among preprocessing stages, noise removal techniques contribute heavily to effective edge identification. This is primarily due to the evolution of state-of-the-art edge-preserving filtering techniques that identify very sensitive edges representing biological structures. From the literature, it is evident that cardiovascular diseases (CVDs) are among the devastating diseases accounting for severe mortality rates worldwide. Several denoising techniques have been investigated to remove noise with special emphasis on alleviating the edges, including median filtering, wavelet-based filtering techniques, nonlocal means, and total variation, along with several other techniques [7–9]. Speckle noise removal in US images was attempted using a bio-inspired variant of genetic programming with a comprehensive analysis of different filtering techniques, including GF, Wiener, and wavelet transform. This implementation was carried out without the need for logarithmic image transformation and threshold values dependent on the individual images [10, 11].

The utility and inevitable need for efficient denoising techniques was emphasized primarily in US images with a comprehensive analysis of edge detection techniques [11]. The importance of efficient denoising techniques, such as curvelet transform-based approaches, to aid in segmenting US CCA structures was explained [5]. Several approaches with mathematical formulations involving partial derivative equations have been proposed exclusively for medical images, including US images [12, 13]. In contrast, state-of-the-art denoising techniques have also been proposed using deep learning strategies for US images [14, 15]. Additionally, several other preprocessing strategies are being developed to aid in formulating effective diagnostic strategies [16, 17]. The effectiveness of state-of-the-art noise removal approaches in performing efficient delineation of tissue of interest in US images with the aid of machine learning approaches indicates the imminent need for edge- and structure-preserving approaches [18]. Designing efficient despeckling techniques in conjunction with enhancement techniques was found to be effective in identifying the intima-media thickness (IMT) in US-based CCA images, which, in turn, paves the way for the early diagnosis of certain CVDs [6]. Designing effective denoising strategies is of paramount interest in early diagnosis related to US-based CCA images. Several of the above approaches were designed to mitigate certain types of noise. Contributing towards efficient pipeline design considering the importance of preserving important structures is the primary goal of this study.

US images are primarily affected by noise, including speckle noise, Gaussian noise, and Poisson noise [4, 7]. B-mode ultrasound images and CCA were primarily used in measuring IMT [4, 19, 20]. In designing and implementing image processing-based pipelines, the results of several processing stages are affected due to the presence of noise. Specific preprocessing methods are essential to mitigating noise and artifacts. Several techniques were employed for identifying plaque present in the ultrasonic images. It is necessary to segment the affected region from the carotid artery ultrasonic image for an accurate diagnosis of carotid plaque. The WNNM filtering technique is very effective in accomplishing the task of removing noise while simultaneously preserving the structural information [20–23]. In this study, different filtering techniques were explored to preserve the CCA structure in US images [24–29]. Major motivation of this study is to identify the usability of filtering techniques to denoise image with clear emphasis to preserve the sensitive structures in the US images. The major limitation of the proposed technique is selecting the proper selection parameters to tune the WNNM filtering technique and the processing time.

3. Proposed Methodology

The input images considered in this study were obtained from carotid artery images. This specific database consists of 84 images related to B-mode ultrasound longitudinal section acquisition of CCA from 10 volunteers [4]. To ensure uniformity and computational ease, images are first resized to 128×128, and next, the resized images are converted to grayscale images. To investigate the filtering capabilities of the filtering techniques, first, the resized grayscale images are corrupted with Gaussian noise of mean and variance of 0 and 0.05, respectively. The flowchart depicting the proposed work is shown in Figure 1.

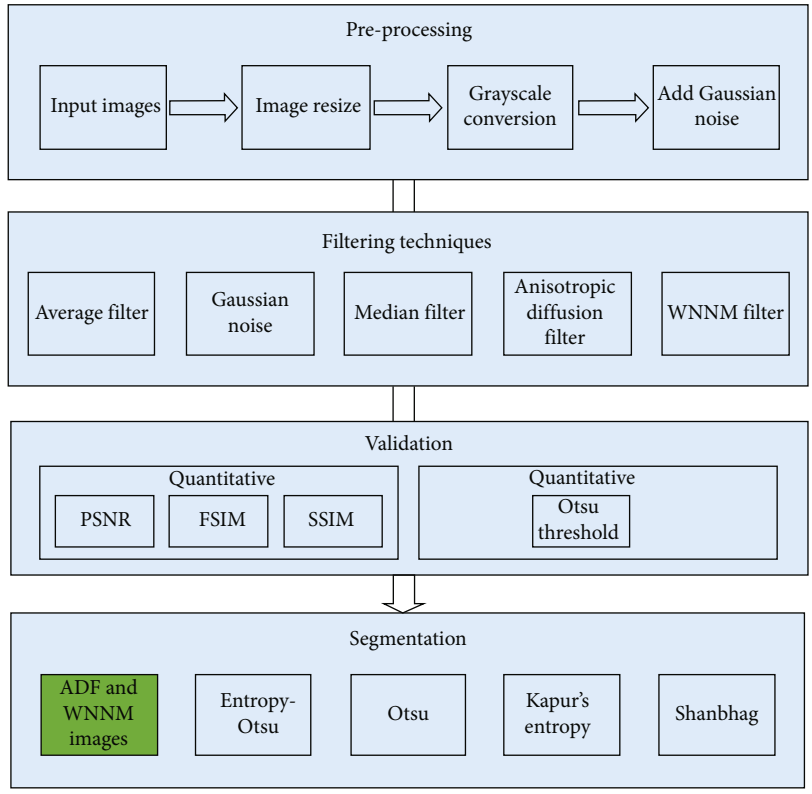

Figure 1: Flowchart representing the proposed approach.

Five denoising techniques, namely, WNNM, anisotropic diffusion filtering (ADF), Gaussian filtering (GF), average filtering (AVGF), and median filtering (MDF), were implemented in this work for CCA image noise removal using MATLAB (2016) [30–32]. Among these five techniques, GF, AVGF, and MDF are conventional filtering techniques, whereas ADF and WNNM operate filtering based on edge information.

3.1. WNNM Filter. The WNNM-based approach utilizes the rank minimization approach, wherein the sum of singular values called the nuclear norm is used for the minimization approach. Soft thresholding utilizing these singular values is further used to perform the filtering operation [20].

$$X^* = \text{argmin}_X f(X) + \tau \|X\|_X. \quad (1)$$

Nuclear norm minimization (NNM) utilized in this approach is expressed as in Equation (1). The function $f(X)$ is defined arbitrarily, and $X \epsilon R^{m*n}$ and τ are regularizing parameters. An improved approximation of the rank minimization was attempted with a weight factor instead of NNM termed weighted nuclear norm minimization (WNNM) [20, 21].

3.2. Anisotropic Diffusion Filter. ADF operates by smoothing the object in such a way that the edges are preserved with the aid of gradient detection, which is given by the equation

$$I_t = \text{div}\,(c(x,y,t)\nabla I) = \frac{\partial}{\partial x}(c(x,y,t)I_x)\frac{\partial}{\partial y}(c(x,y,t)I_y), \quad (2)$$

where c is the conduction diffusion coefficient which is responsible for performing the smoothing operation on the image, whereas I_x and I_y are image gradients observed in the x and y directions, respectively. The c is considered as a function representing the magnitude of gradient of brightness function f given by

$$c(x,y,t) = f(\|\nabla I(x,y,t)\|). \quad (3)$$

In order to preserve the edges, proper selection of the function f is essential. The commonly used function for diffusivity f is given by

$$f(\|\nabla I(x,y,t)\|) = \exp\left(-\left(\frac{\|\nabla I\|}{K}\right)^2\right), \quad (4)$$

where K is a constant called as kappa and represents the edge strength threshold [30, 31]. GF, AVGF, and MDF were implemented with window sizes of (3, 3) [32, 33].

The equations to represent validation metrics are shown in Table 1, where f_{flt} is the filtered image, $f_{\text{org}}$is the original image, $M\mu_{f_{\text{org}}}$, $\sigma^2_{f_{\text{org}}}$, $\mu_{f_{\text{flt}}}$, $\sigma^2_{f_{\text{flt}}}$ are the mean and variance of filtered and original images, $\sigma_{f_{\text{org}},ff_{lt}}$ is the covariance between the original and filtered images, and c_1 and c_2 are constants. PC (x) is phase congruency computed for image, and $S(x)$ is similarity between two images. MSE is mean square error.

Validation is performed with the aid of metrics such as PSNR, SSIM, and FSIM [22–26, 34–38]. The main objective

Input: Noisy image x
1. Initialize x_0, y_0
2. For $k = 1$ to n number of iterations
3. Regularize in each iteration
4. For each patch in the image of fixed size
5. Identify identical patch group
6. Estimate weight vector
7. Perform singular value decomposition (SVD)
8. Obtain the estimate X_j
9. End
10. Build clean image at the iteration k
11. End
Output: Filtered image x_{filt}

Algorithm 1

Table 1: Validation measures and formulae.

Measures	Formulae
PSNR	$PSNR\left(f_{\text{flt}}, f_{\text{org}}\right) = 10 \log\left(255^2/\text{MSE}\left(f_{\text{flt}}, f_{\text{org}}\right)\right)$
FSIM	$\text{FSIM}\left(f_{\text{flt}}, f_{\text{org}}\right) = \frac{\sum S(x).PC(x)}{(\sum PC(x))}$
SSIM	$\text{SSIM}\left(f_{\text{flt}}, f_{\text{org}}\right) = \frac{1}{M}\sum \frac{\left(2\mu_{f_{\text{org}}}\mu_{f_{\text{flt}}} + c_1\right)\left(2\sigma_{f_{\text{org}}, f_{\text{flt}}} + c_2\right)}{\left(\mu^2_{f_{\text{org}}} + \mu^2_{f_{\text{flt}}} + c_1\right)\left(\sigma^2_{f_{\text{org}}} + \sigma^2_{f_{\text{flt}}} + c_2\right)}$

of the study is to investigate the performance of the filtering techniques to preserve the fine structures and segment the structures. Histograms of the images are also investigated in the process of validating the efficacy of the WNNM filtering approach over other techniques. Validating the segmentation is not the focus of the study [39]. The edge-based filtering techniques such as ADF and WNNM were discussed in the paper to identify the efficacy of the work. The Meta-heuristic based segmentation approaches such as Otsu-based thresholding, Kapur's entropy and Shanbhag entropy were also attempted in this paper for investigation of the proposed work. The tools used in the work are Python3.7, OpenCV, and Skimag libraries [22–29, 32, 37, 38, 40–53].

From the above equations:

(i) Otsu: Here, i and j represent indices for the two intensity classes, namely, foreground and background; ω_i is the probability of occurrence, and μ_i is the mean of a class, respectively. This method operates by selecting the optimal threshold by means of maximizing the objective function using the equation and the interclass variance between the classes

(ii) Kapur's entropy: In this approach, the optimal threshold is computed based on the maximum entropy defined by the equation, where $H(\rho_i)$ is the Shannon's entropy of the corresponding class

(iii) Shanbhag entropy: In this approach, the membership value is assigned to the pixel intensities based on their proximity to the class threshold as defined by the equation

Figure 1 shows the flowchart representation of the proposed denoising method. In Figure 1(a), the input images are prepared before noise removal. Later, five individual filters were applied to the noisy images to obtain filtered images. In Figure 1(b), the filtered images were first subjected to validation, followed by Otsu-based threshold and morphological operation.

4. Results and Discussion

The representative CCA image used from the dataset is shown in Figure 2(a). In Figure 2(b), the representative image, which is resized to a 128×128 matrix size, converted to grayscale and corrupted with Gaussian noise, is shown. It can be observed that the presence of noise has a severe impact on identifying CCA structural information.

Images filtered using different filtering techniques are shown in Figure 3. In Figure 3(a), a noisy image filtered using an average filter is shown. The influence of the filtering technique is visible primarily in certain regions, especially pixels representing low-intensity levels with sizeable, localized regions, but noise is still predominant in the structures. In Figure 3(b), the Gaussian-filtered image is shown, in which it can be seen that the presence of noise is observed

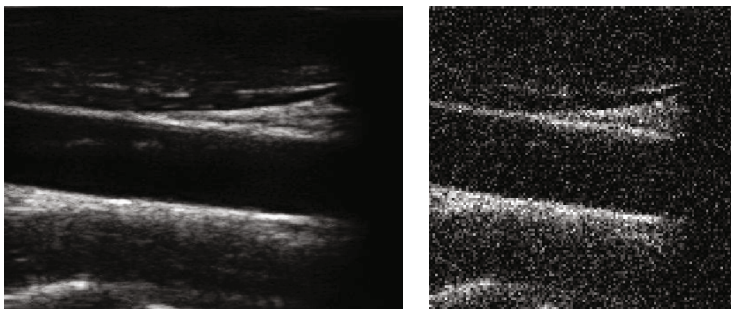

(a) (b)

Figure 2: Representative and resized CCA image: (a) input image and (b) image resized and noise corrupted image.

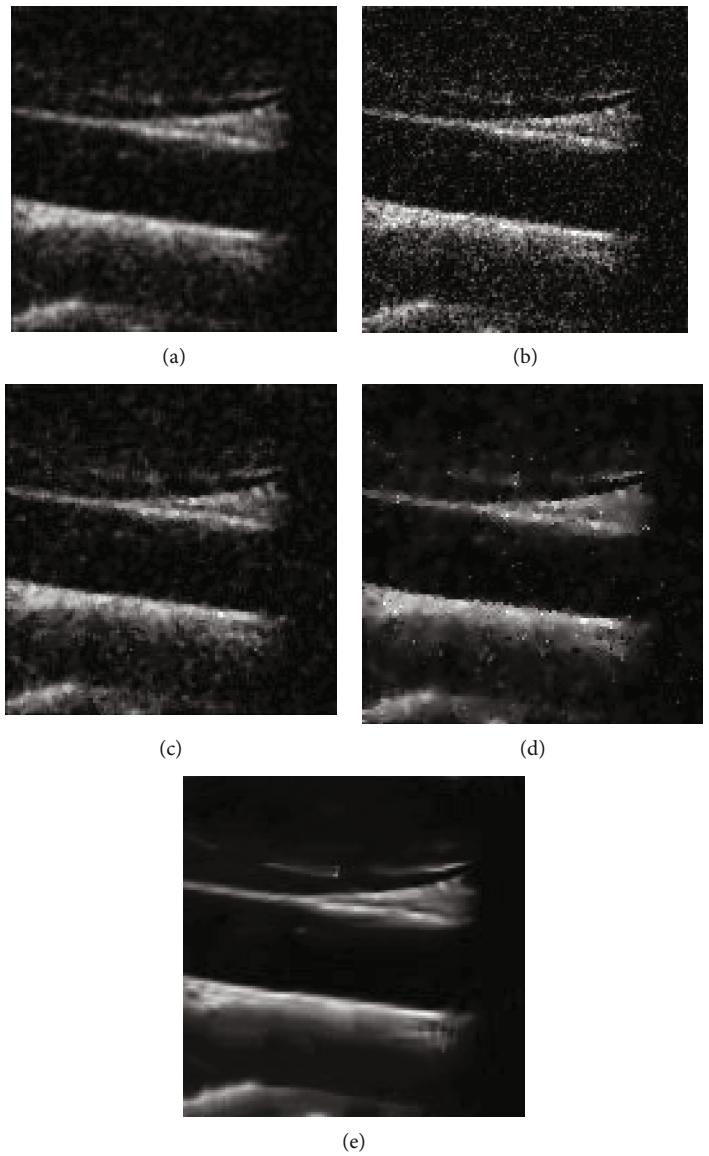

(a) (b)

(c) (d)

(e)

Figure 3: Filtered images. (a) Average filtered, (b) Gaussian filtered, (c) median filtered, (d) anisotropic filtered, and (e) WNNM filtered.

throughout the image. The median-filtered image is shown in Figure 3(c), and the noise seems to be marginally reduced. An anisotropic filtered image is shown in Figure 3(d), and the technique seems to have filtered the noise with due importance to edges, such as retaining structure. However, some of the sensitive structures seem to be blurred. The WNNM-filtered image shown in Figure 3(e) appears to have removed noise while preserving the important structures.

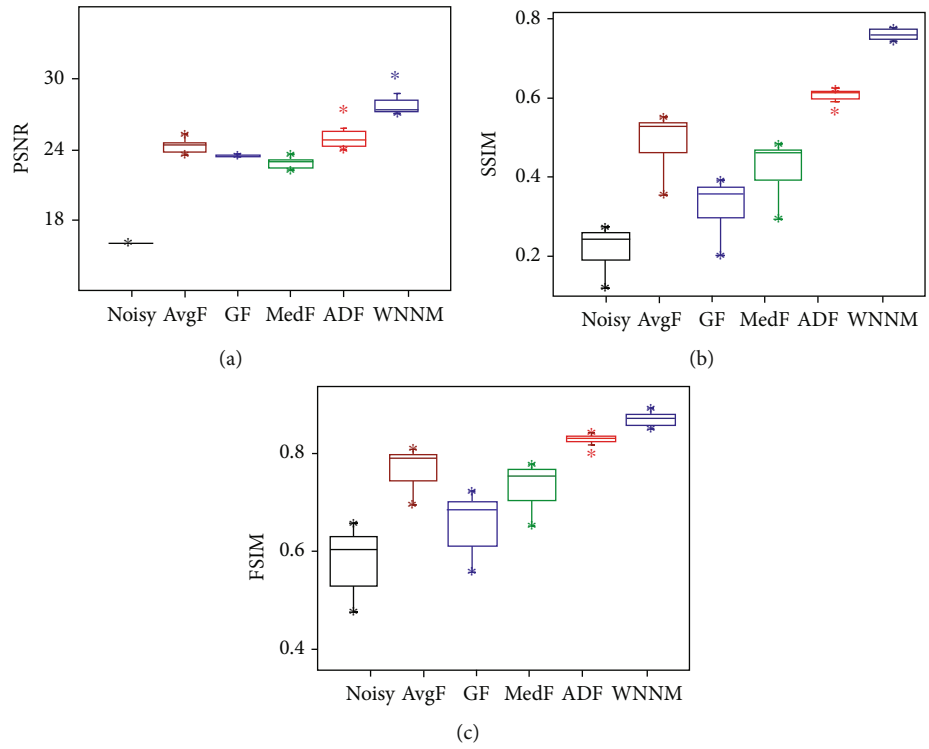

Figure 4: Boxplot representation of validation metrics for different filtering techniques: (a) PSNR, (b) SSIM, and (c) FSIM.

The box plot representation of the validation metrics, such as PSNR, SSIM, and FSIM, is shown in Figure 4. The PSNR of the noisy images and the filtered images is shown in Figure 4(a). It can be observed that noisy images have very low PSNR, and all the filtering techniques contributed to removing noise and improving PSNR with clear variations seen across the techniques. The PSNR in the case of ADF and WNNM appears to be better compared to conventional filtering techniques. Among ADF and WNNM, the performance of WNNM is clearly seen to be better with higher PSNR values.

The SSIM-based plot is shown in Figure 4(b). A similar trend can be seen with a much higher (greater than 0.7) SSIM value obtained with WNNM among all the filtering techniques. The next best performance is observed in the case of ADF, which also has low variance. SSIM values for all the conventional filtering techniques are less than 0.6, which also has a very high variance. Additionally, the SSIM values for noisy images are far lower (less than 0.3).

The FSIM-based box plot comparison is shown in Figure 4(c). The FSIM values indicate that there appears to be a marginal improvement in the case of AVGF and MDF, whereas slightly better performance can be seen in the case of GF and ADF. GF-based FSIM values have high variation. FSIM values in the case of WNNM are higher than those of the rest of the filtering techniques. Additionally, the low variance achieved by WNNM and ADF techniques is observed.

Histograms of the input image, noisy image, and filtered images using different techniques are depicted in Figure 5. The histogram of the input image is shown in Figure 6(a), where it can be observed that the histogram is skewed left with the majority of the intensities concentrated close to low-intensity levels. The histogram of the noisy image in Figure 6(b) indicates that the added noise spread the intensities across and depicted the near Gaussian curve morphology. The histogram of the Gaussian-filtered image in Figure 6(c) clearly indicates that the morphology of the Gaussian curve is still intact, which means that the filtering is not instrumental in making the image closely resemble the input image. The histogram of the median-filtered image in Figure 6(d) indicates that the spread is relatively reduced but still not close enough to depict the morphology of the input image. The average filter performance also seems to reduce the spread marginally, as depicted in Figure 6(e). The spread in the intensity levels is considerably reduced after the image is filtered using an anisotropic diffusion filter, as represented by the histogram in Figure 6(f). The histogram of the WNNM-filtered image in Figure 6(g) seems to closely resemble the histogram in that of the input image, shown in Figure 6(a).

The values obtained using validation metrics such as PSNR, SSIM, and FSIM are depicted in Table 2. The metric values in the noisy images prove that the influence of noise degrades the image quality. The PSNR values are considerably improved with WNNM and ADF compared to conventional filtering techniques. Similar trends are observed in the SSIM and FSIM measures. The system specifications are Windows 10, 64-bit OS, 2.00GHz processor and 4GB RAM.

The results obtained in this study clearly indicate that image smoothing filters, which have a clear mechanism to smooth the pixels and regions representing nonedge

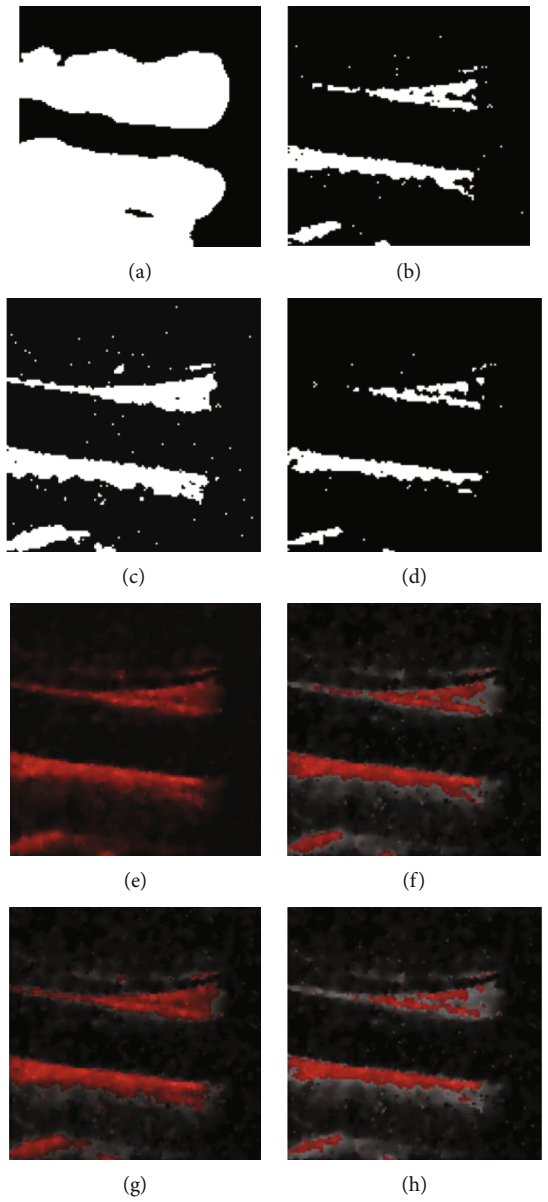

Figure 5: Segmentation masks of ADF images and mask overlay: (a) entropy-Otsu threshold, (b) Otsu threshold, (c) Kapur's entropy, (d) Shanbhag entropy segmentation, and (e)–(h) overlay of (a)–(d).

information while enhancing the regions representing edges, are important for US images. Two of the conventional filters, GF and AVGF, generally operate the process of removing noise without considering the nature of regions, especially without bothering whether the regions represent edges. The performance of these filters is moderate, as depicted by the quantitative measures. MDF, which operates based on the median value in the mask region, is moderate with respect to SSIM but overall does not provide significant results. ADF is an edge-preserving filter that operates by identifying the edge representing pixels, wherein based on the lambda value, the smoothing is high in nonedge regions. The filtering results are better than those of most conventional filters. The formulae for Entropy and segmentation approaches are incorporated in Table 3.

The computation times are more for ADF and WNNM. But, the medical image analysis requires accuracy. Thus, ADF and WNNM considered for the biomedical applications and are incorporated in Table 4.

The results rendered by the WNNM filtering technique, which operates based on singular values, are impressive, as suggested by quantitative measures as well as qualitative observations. A high SSIM clearly indicates that the structure of the image before adding noise was retrieved after filtering. It can be inferred that the WNNM filtering technique can be used in designing an effective preprocessing module in US-based CCA images. The importance of noise removal using different approaches and their impact on segmenting specific tissue in US images as depicted in several studies is found to be interesting and much needed [1, 2]. In this

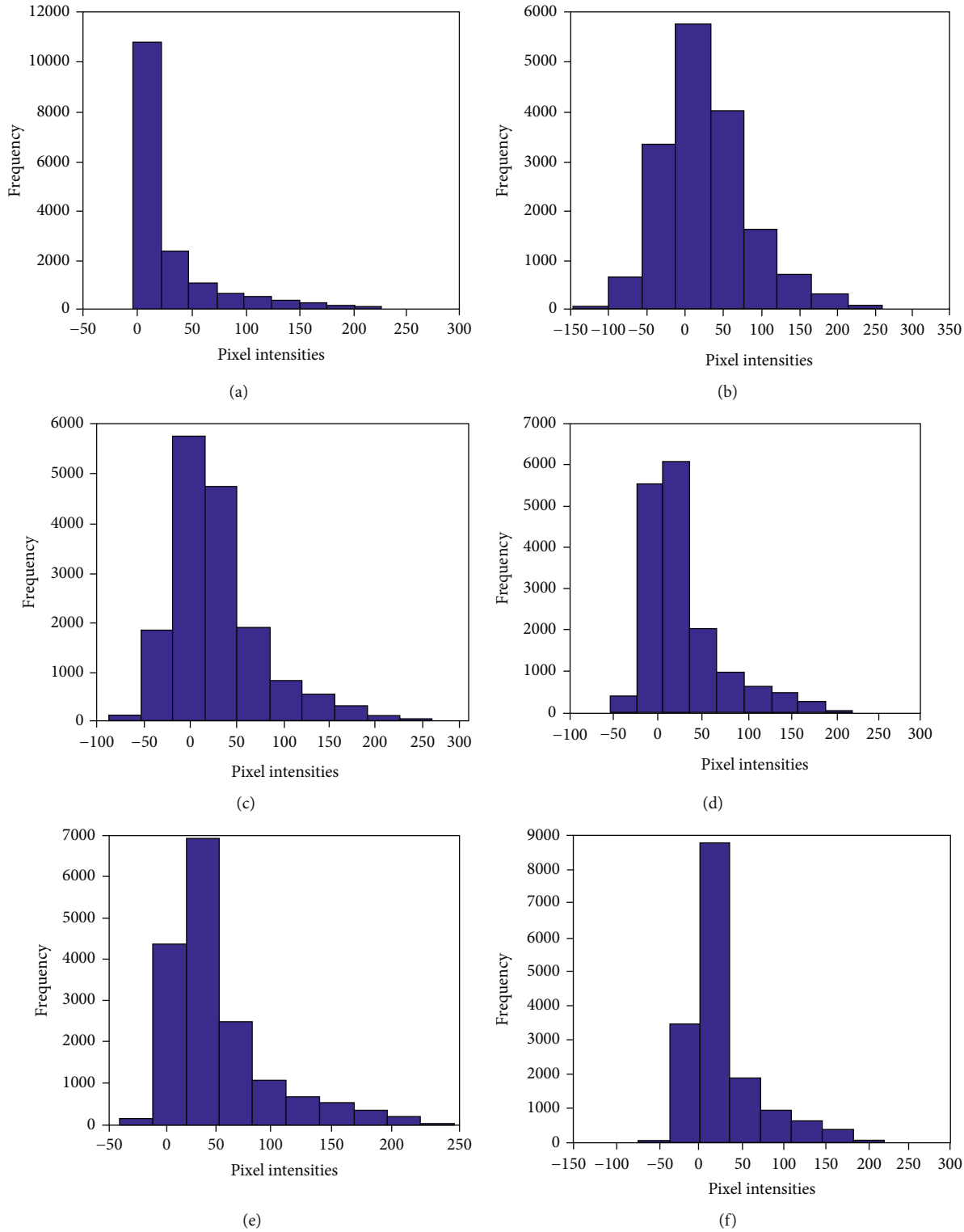

Figure 6: Continued.

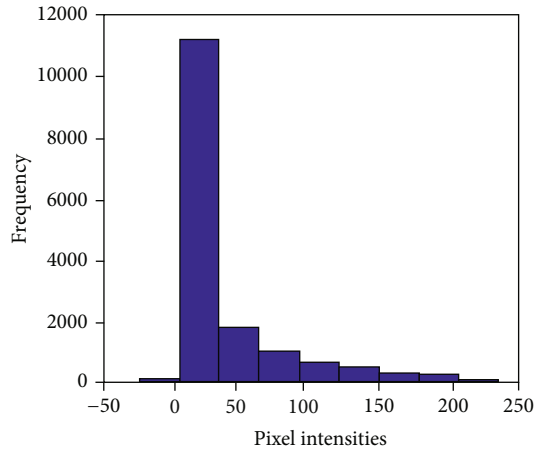

(g)

Figure 6: Histograms of input, noisy, and filtered images: (a) input image, (b) noisy version of (a), (c) Gaussian filter filtered, (d) median filtered, (e) average filtered, (f) anisotropic diffusion filtered, and (g) WNNM filtered; x-axis represents pixel intensity, and y-axis represents the frequency or count of the pixel intensities.

Table 2: Comparison of validation metrics of different filtering techniques.

Validation measures	Noisy images	Filtering techniques				
		GF	AVGF	MDF	ADF	WNNM
PSNR	16.02 ± 0.00	23.49 ± 0.04	24.29 ± 0.48	22.85 ± 0.36	25.01 ± 0.91	27.84 ± 1.04
SSIM	0.22 ± 0.04	0.33 ± 0.06	0.50 ± 0.06	0.43 ± 0.06	0.61 ± 0.02	0.76 ± 0.01
FSIM	0.27 ± 0.05	0.66 ± 0.06	0.77 ± 0.04	0.74 ± 0.04	0.83 ± 0.01	0.87 ± 0.01

Significance level: P value <0.0001 results for all metrics across filtering techniques w.r.t. noisy images.

Table 3: Entropy and segmentation approaches with formulae.

Measures	Formulae
Entropy	$H = \sum_i x_i \log(x_i)$
Otsu threshold	$\sigma^{2c} = \sum_{i,j} w_i w_j \left(\mu_i - \mu_j\right)^2$
Kapur's entropy	$\arg\max \sum_{i=0}^{M-1} H(\rho_i)$
Shanbhag entropy	$H_f(T) = \sum_{g=T+1}^{G} \frac{p(g)}{1-P(T)} \log[\mu_o(g)]$

Table 4: Comparison of Computing times.

Filtering techniques	Computation time (in sec)
Gaussian filter(GF)	0.01
Average filter (AVGF)	0.01
Median filter (MDF)	0.3
Anisotropic diffusion filter (ADF)	0.4
Weighted nuclear norm minimization (WNNM)	32

study, the basic segmentation strategy, namely, Otsu-based thresholding, is used to delineate the tissue. Additionally, no validation strategy for segmentation is implemented. Hence, the use of state-of-the-art segmentation approaches along with validation measures is a definite scope for future enhancements in related studies.

The three validation metrics, namely, PSNR, SSIM, and FSIM, clearly indicate that the two edge-preserving filters, ADF and WNNM, are performed better than the conventional filter.

To further investigate the quantitative analysis, the entropy-based segmentation techniques were used to compare the ADF and WNNM.

The segmented masks obtained using entropy-Otsu, Otsu thresholding, Kapur's entropy, and Shanbhag entropy are shown in Figure 7 for ADF images in first row and corresponding overlay in the second row. The Otsu threshold entropy images in (a) indicate oversegmentation performed by the method. The Otsu thresholding in (b) and Shanbagh-based segmentation in (d) seem to have performed moderately to segment the boundaries of CCA. On the other hand, the Kapur's entropy-based mask in (c) has been observed to have performed relatively better to delineate the intended structures. The metrics of different filtering techniques are compared in Table 2.

The segmented masks and overlays obtained after filtering the images with WNNM-based filter are shown in Figure 7. The Otsu threshold entropy images in (a) again

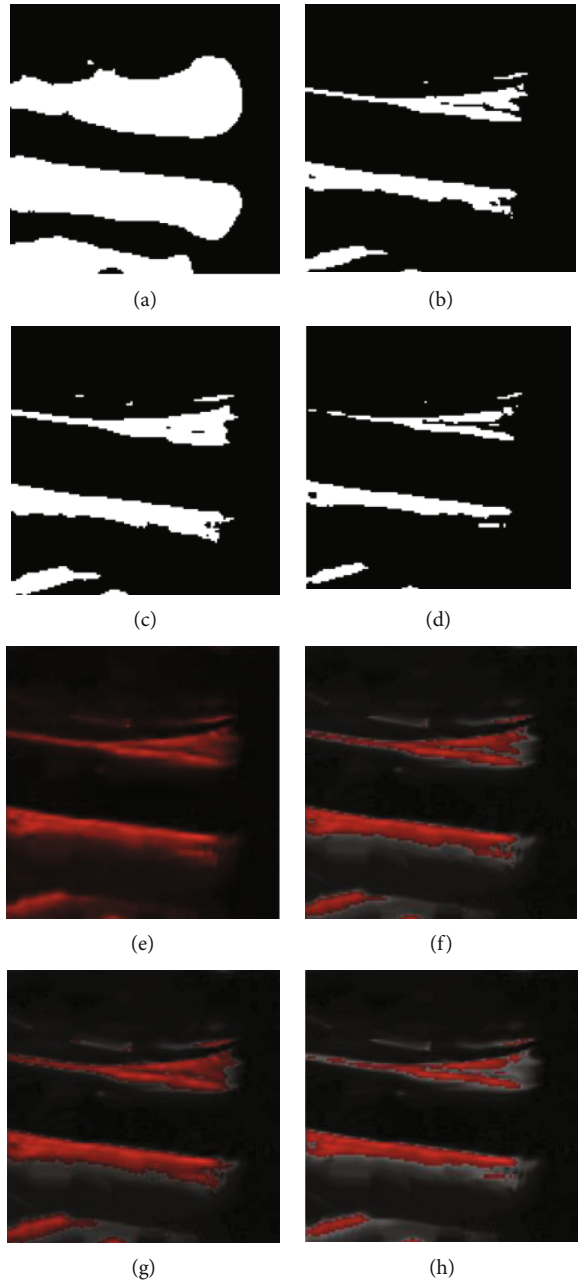

Figure 7: Segmentation masks of WNNM images and mask overlay: (a) entropy-Otsu threshold, (b) Otsu threshold, (c) Kapur's entropy, (d) Shanbhag entropy, and (e)–(h) overlay of (a)–(d).

indicate oversegmentation. The Otsu thresholding in (b) and Shanbagh-based segmentation in (d) seem to have performed again moderately to segment the boundaries of CCA. The Kapur's entropy-based mask in (c) has been found to have resulted in better delineating the structures.

5. Discussions

The presence of noise in ultrasound images severely affects image quality, thereby leading to difficulty in the efficient design of image processing-based diagnostic tools. Primarily, noise impacts the CCA structure morphology, as they are defined with sensitive edges. Even small noise can be detrimental to effective CVD diagnosis. High efficacy resulting design strategies are of paramount importance to alleviating edges and preventing the smoothing of very sensitive edges constituting structures of interest. We carried out a comprehensive qualitative and quantitative analysis by implementing five different filtering techniques collaborating with validation metrics. Furthermore, the filtered images were segmented to perform a qualitative analysis of the denoising approaches. It was found that the WNNM removed the noise as evident from the high validation metric values and further supported by the segmentation results, which had fewer noisy structures. ADF, which is an edge-enhancing filtering technique, also provided better

validation metrics. Conventional filtering approaches that were performed in the closest vicinity could not reduce the impact of noise and induce noisy structures.

Histogram-based validation also suggests that the WNNM filter was instrumental in reducing noise and restoring the histogram close to the input image. Histogram-based validation further reiterates that the WNNM filter is robust in many aspects for providing efficient noise reduction. Hence, WNNM can be a very useful filtering technique for alleviating and preserving tissue structures. Various approaches of obtaining threshold using entropy-based information further provide wider ability of the preprocessing, especially the edge-preserving filters to aid in near optimal segmentation of the CCA which is very essential to aid in the diagnosis of the IMT and possible presence of the plaque.

6. Conclusion

Designing a comprehensive methodology requires efficiently designing each module starting from preprocessing; hence, this study aims to contribute to this field and to include machine learning approaches in various modules. This paper proves quite useful in aiding clinical experts, including radiologists, in their clinical investigations followed by diagnosis. This approach may further lead to future investigations involving structural preservation in real-time situations and denoising ultrasound images.

Data Availability

The data used in this paper are available from the corresponding author upon request.

Conflicts of Interest

The authors declare that they have no conflicts of interest regarding this work.

Acknowledgments

The authors would like to thank the support of the Deanship of Scientific Research at Princess Nourah bint Abdulrahman University. This research was funded by Princess Nourah bint Abdulrahman University Researchers Supporting Project number (PNURSP2022R239), Princess Nourah bint Abdulrahman University, Riyadh, Saudi Arabia.

References

[1] K. L. Weind, C. F. Maier, B. K. Rutt, and M. Moussa, "Invasive carcinomas and fibroadenomas of the breast: comparison of microvessel distributions–implications for imaging modalities," *Radiology*, vol. 208, no. 2, pp. 477–483, 1998.

[2] R. R. Entrekin, B. A. Porter, H. H. Sillesen, A. D. Wong, P. L. Cooperberg, and C. H. Fix, "Real-time spatial compound imaging: application to breast, vascular, and musculoskeletal ultrasound," in *Seminars in Ultrasound, CT and MRI*, vol. 22, no. 1pp. 50–64, WB Saunders, 2001.

[3] D. D. Adler, P. L. Carson, J. M. Rubin, and D. Quinn-Reid, "Doppler ultrasound color flow imaging in the study of breast cancer: preliminary findings," *Ultrasound in medicine & biology*, vol. 16, no. 6, pp. 553–559, 1990.

[4] M. Zukal, R. Beneš, P. Číka, and K. Říha, "Towards an optimal interest point detector for measurements in ultrasound Images," *Measurement Science Review*, vol. 13, no. 6, pp. 329–338, 2013.

[5] L. Subbiah, D. Samiappan, and P. Muthu, "Automated denoised ultrasound carotid artery image segmentation using curvelet threshold decomposition," in *2017 International Conference on Wireless Communications, Signal Processing and Networking (WiSPNET)*, Chennai, India, 2017.

[6] Y. Nagaraj, P. Madipalli, J. Rajan, P. K. Kumar, and A. V. Narasimhadhan, "Segmentation of intima media complex from carotid ultrasound images using wind driven optimization technique," *Biomedical Signal Processing and Control*, vol. 40, pp. 462–472, 2018.

[7] F. Benzarti and H. Amiri, "Speckle noise reduction in medical ultrasound images," pp. 1305–1344, 2013, https://arxiv.org/pdf/1305.1344.

[8] C. M. J. M. Dourado, S. P. P. da Silva, R. V. M. da Nobrega, P. P. Rebouças Filho, K. Muhammad, and V. H. C. de Albuquerque, "An open IoHT-based deep learning framework for online medical image recognition," *IEEE Journal on Selected Areas in Communications*, vol. 39, no. 2, pp. 541–548, 2021.

[9] Y. Nagaraj, C. S. Asha, and A. V. Narasimhadhan, "Assessment of speckle denoising in ultrasound carotid images using least square Bayesian estimation approach," in *2016 IEEE Region 10 Conference (TENCON)*, Singapore, 2016.

[10] S. M. Mahbubur Rahman, M. Omair Ahmad, and M. N. S. Swamy, "Wavelet-domain image denoising algorithm using series expansion of coefficient p.d.f. in terms of Hermite polynomials," in *Proceedings of 3rd International IEEE North-East Workshop on Circuits and Systems*, pp. 271–275, Quebec City, QC, Canada, 2005.

[11] P. P. Rebouças Filho, P. C. Cortez, A. C. da Silva Barros, and V. H. De Albuquerque, "Novel adaptive balloon active contour method based on internal force for image segmentation - a systematic evaluation on synthetic and real images," *Expert Systems with Applications*, vol. 41, no. 17, pp. 7707–7721, 2014.

[12] M. A. Kabir and C. Shahnaz, "An ECG signal denoising method based on enhancement algorithms in EMD and Wavelet domains," in *TENCON 2011-2011 IEEE Region 10 Conference*, pp. 284–287, Bali, Indonesia, 2011.

[13] C. M. Dourado Jr., S. P. da Silva, R. V. da Nobrega, A. C. Barros, P. P. Reboucas Filho, and V. H. de Albuquerque, "Deep learning IoT system for online stroke detection in skull computed tomography images," *Computer Networks*, vol. 152, pp. 25–39, 2019.

[14] S. G. Javed, A. Majid, and Y. S. Lee, "Developing a bio-inspired multi-gene genetic programming based intelligent estimator to reduce speckle noise from ultrasound images," *Multimedia Tools and Applications*, vol. 77, no. 12, pp. 15657–15675, 2018.

[15] P. Tiwari, J. Qian, Q. Li et al., "Detection of subtype blood cells using deep learning," *Cognitive Systems Research*, vol. 52, pp. 1036–1044, 2018.

[16] Y. Nagaraj and A. V. Narasimhadhan, "Comparison of edge detection algorithms in the framework of despeckling carotid ultrasound images based on bayesian estimation approach," in *National Conference on Computer Vision, Pattern Recognition, Image Processing, and Graphics-Springer*, Singapore, 2018.

[17] A. Hadri, L. Afraites, A. Laghrib, and M. Nachaoui, "A novel image denoising approach based on a non-convex constrained

PDE: application to ultrasound images," *Signal, Image and Video Processing*, vol. 15, no. 5, pp. 1057–1064, 2021.

[18] H. Houichet, A. Theljani, and M. Moakher, "A nonlinear fourth-order PDE for image denoising in Sobolev spaces with variable exponents and its numerical algorithm," *Computational and Applied Mathematics*, vol. 40, no. 3, pp. 1–29, 2021.

[19] F. Sadik, A. G. Dastider, and S. A. Fattah, "SpecMEn-DL: spectral mask enhancement with deep learning models to predict COVID-19 from lung ultrasound videos," *Health Information Science and Systems*, vol. 9, no. 1, pp. 1–11, 2021.

[20] T. Mahmud, S. A. Fattah, and M. Saquib, "Deeparrnet: an efficient deep cnn architecture for automatic arrhythmia detection and classification from denoised ecg Beats," *Access*, vol. 8, pp. 104788–104800, 2020.

[21] Z. Gao, X. Wang, S. Sun et al., "Learning physical properties in complex visual scenes: an intelligent machine for perceiving blood flow dynamics from static CT angiography imaging," *Neural Networks*, vol. 123, pp. 82–93, 2020.

[22] S. Gu, L. Zhang, W. Zuo, and X. Feng, "Weighted nuclear norm minimization with application to image denoising," in *IEEE Conference on Computer Vision and Pattern Recognition (CVPR)*, pp. 2862–2869, Columbus, OH, USA, 2014.

[23] S. Gu, Q. Xie, D. Meng, W. Zuo, X. Feng, and L. Zhang, "Weighted nuclear norm minimization and its applications to low level vision," *International Journal of Computer Vision*, vol. 121, no. 2, pp. 183–208, 2017.

[24] K. R. Anandh, C. M. Sujatha, and S. Ramakrishnan, "Atrophy analysis of corpus callosum in Alzheimer brain MR images using anisotropic diffusion filtering and level sets," in *2014 36th Annual International Conference of the IEEE Engineering in Medicine and Biology Society*, Chicago, IL, USA, 2014.

[25] S. S. Suganthi and S. Ramakrishnan, "Anisotropic diffusion filter based edge enhancement for segmentation of breast thermogram using level sets," *Biomedical Signal Processing and Control*, vol. 10, pp. 128–136, 2014.

[26] K. Shankar, A. R. W. Sait, D. Gupta, S. K. Lakshmanaprabu, A. Khanna, and H. M. Pandey, "Automated detection and classification of fundus diabetic retinopathy images using synergic deep learning model," *Pattern Recognition Letters*, vol. 133, pp. 210–216, 2020.

[27] M. Sezgin and B. Sankur, "Survey over image thresholding techniques and quantitative performance evaluation," *Journal of Electronic Imaging*, vol. 13, no. 1, pp. 146–165, 2004.

[28] G. T. Reddy, M. P. K. Reddy, K. Lakshmanna, D. S. Rajput, R. Kaluri, and G. Srivastava, "Hybrid genetic algorithm and a fuzzy logic classifier for heart disease diagnosis," *Evolutionary Intelligence*, vol. 13, no. 2, pp. 185–196, 2020.

[29] D. Oliva, M. A. Elaziz, and S. Hinojosa, *Metaheuristic Algorithms for Image Segmentation: Theory and Applications*, Springer International Publishing, 2019.

[30] N. Biradar, M. L. Dewal, and M. K. Rohit, "A novel hybrid homomorphic fuzzy filter for speckle noise reduction," *Biomedical Engineering Letters*, vol. 4, no. 2, pp. 176–185, 2014.

[31] S. K. Avuti, V. Bajaj, A. Kumar, and G. K. Singh, "A novel pectoral muscle segmentation from scanned mammograms using EMO algorithm," *Biomedical Engineering Letters*, vol. 9, no. 4, pp. 481–496, 2019.

[32] E. F. Ohata, G. M. Bezerra, J. V. S. das Chagas et al., "Automatic detection of COVID-19 infection using chest X-ray images through transfer learning," *IEEE/CAA Journal of Automatica Sinica*, vol. 8, no. 1, pp. 239–248, 2021.

[33] P. Muthukumar, "Chaos.: synchronization and digital image enhancement technique based on a novel 5D fractional-order hyperchaotic memristive system," *Circuits, Systems, and Signal Processing*, vol. 41, pp. 2266–2289, 2022.

[34] D. Gupta, J. Arora, U. Agrawal, A. Khanna, and V. H. C. de Albuquerque, "Optimized binary Bat algorithm for classification of white blood cells," *Measurement*, vol. 143, pp. 180–190, 2019.

[35] M. A. Kabir and C. Shahnaz, "Comparison of ECG signal denoising algorithms in EMD and wavelet domains," *IJRRAS*, vol. 11, no. 3, pp. 499–516, 2012.

[36] X. Yang, C. Wu, D. Zhou, and T. Li, "Fast image super-resolution based on limit gradient embedding cascaded Forest," *Circuits, Systems, and Signal Processing*, vol. 41, no. 4, pp. 2007–2026, 2022.

[37] M. Ashfanoor Kabir and C. Shahnaz, "Denoising of ECG signals based on noise reduction algorithms in EMD and wavelet domains," *Biomedical Signal Processing and Control*, vol. 7, no. 5, pp. 481–489, 2012.

[38] I. Mehmood, A. Ullah, K. Muhammad et al., "Efficient image recognition and retrieval on IoT-assisted energy-constrained platforms from big data repositories," *IEEE Internet of Things Journal*, vol. 6, no. 6, pp. 9246–9255, 2019.

[39] S. F. Qadri, L. Shen, M. Ahmad, S. Qadri, S. S. Zareen, and S. Khan, "OP-convNet: a patch classification-based framework for CT vertebrae segmentation," *IEEE Access*, vol. 9, pp. 158227–158240, 2021.

[40] Y. Nagaraj, C. S. Asha, and A. V. Narasimhadhan, "Carotid wall segmentation in longitudinal ultrasound images using structured random forest," *Computers & Electrical Engineering*, vol. 69, pp. 753–767, 2018.

[41] R. H. Selzer, H. N. Hodis, H. Kwong-Fu et al., "Evaluation of computerized edge tracking for quantifying intima-media thickness of the common carotid artery from B-mode ultrasound images," *Atherosclerosis*, vol. 111, no. 1, pp. 1–11, 1994.

[42] M. A. Khan, K. Muhammad, M. Sharif, T. Akram, and V. H. C. . Albuquerque, "Multi-class skin lesion detection and classification via teledermatology," *IEEE Journal of Biomedical and Health Informatics*, vol. 25, no. 12, pp. 4267–4275, 2021.

[43] G. V. Prateek, Y. E. Ju, and A. Nehorai, "Sparsity-assisted signal denoising and pattern recognition in time-series data," *Signal Processing*, vol. 41, no. 1, pp. 249–298, 2022.

[44] P. S. Parvaze and S. Ramakrishnan, "Extraction of multiple cellular objects in HEp-2 images using LS segmentation," *IEIE Transactions on Smart Processing & Computing*, vol. 6, no. 6, pp. 401–408, 2017.

[45] A. P. S. Susaiyah, S. P. Pathan, and R. Swaminathan, "Classification of indirect immunofluorescence images using thresholded local binary count features," *Biomedical Engineering*, vol. 2, no. 1, pp. 479–482, 2016.

[46] H. Ullah, K. Muhammad, M. Irfan, S. Anwar, M. S. A. S. Imran, and V. H. C. de Albuquerque, "Light-dehaze net: a novel lightweight CNN architecture for single image dehazing," *IEEE Transactions on Image Processing*, vol. 30, pp. 8968–8982, 2021.

[47] P. S. Parvaze and S. Ramakrishnan, "Track O. image computing," *Biomedical Engineering/Biomedizinische Technik*, vol. 61, no. s1, pp. 137–178, 2016.

[48] D. Dansana, R. Kumar, A. D. J. Bhattacharjee, D. G. Hemanth, A. Khanna, and O. Castillo, "Early diagnosis of COVID-19-affected patients based on X-ray and computed tomography

images using deep learning algorithm," *Soft Computing*, vol. 24, no. 16, pp. 1–9, 2020.

[49] S. Van der Walt, J. L. Schönberger, J. Nunez-Iglesias et al., "Scikit-image: image processing in python," *Peer J*, vol. 2, article e453, 2014.

[50] P. Sivananthamaitrey and P. R. Kumar, "Optimal dual watermarking of color images with SWT and SVD through genetic algorithm," *Circuits Syst Signal Process*, vol. 41, no. 1, pp. 224–248, 2022.

[51] M. Abd Elaziz, A. A. Ewees, D. Yousri et al., "An improved marine predators algorithm with fuzzy entropy for multilevel thresholding: real world example of COVID-19 CT image segmentation," *IEEE Access*, vol. 8, pp. 125306–125330, 2020.

[52] D. Yousri, M. Abd Elaziz, L. Abualigah, D. Oliva, M. A. A. al-qaness, and A. A. Ewees, "COVID-19 X-ray images classification based on enhanced fractional-order cuckoo search optimizer using heavy-tailed distributions," *Applied Soft Computing*, vol. 101, article 107052, 2021.

[53] K. H. Abdulkareem, M. A. Mohammed, A. Salim et al., "Realizing an effective COVID-19 diagnosis system based on machine learning and IOT in smart hospital environment," *IEEE Internet of Things Journal*, vol. 8, no. 21, pp. 15919–15928, 2021.